SUPPLEMENTARY FIGURES

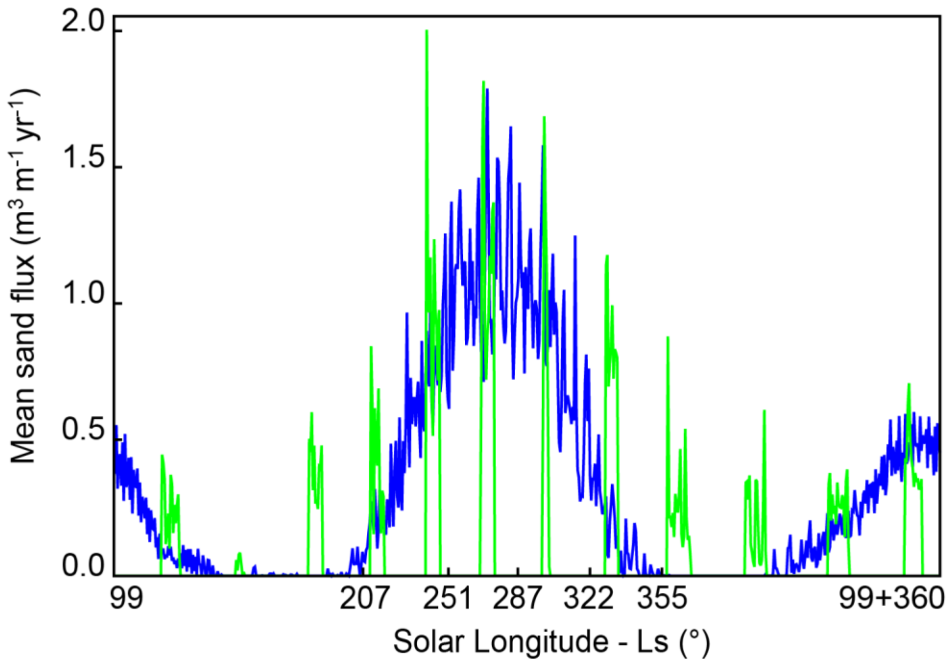

Supplementary Figure 1: Comparison between GCM and mesoscale sand fluxes predictions (using the Lettau and Lettau (1978)[38] transport law, and a stress threshold of 0.01 N m^{-2}). GCM flux prediction (blue) was simulated every minute for a continuous Mars year, on a 2° resolution grid. Mesoscale flux prediction (green) was simulated every minute for 5-10 continuous days every 30° Ls, on a 1.5 km resolution grid. Both predictions display similar seasonal variation amplitude, suggesting 1) that most of the wind drivers are captured in the GCM in Nili Patera area, and 2) that the stress threshold estimated from the GCM would be in the same range as the stress threshold determined from the mesoscale. Note that on this graph, the mesoscale prediction has been linearly scaled (preserving the relative temporal variation) to allow comparison with the GCM prediction.

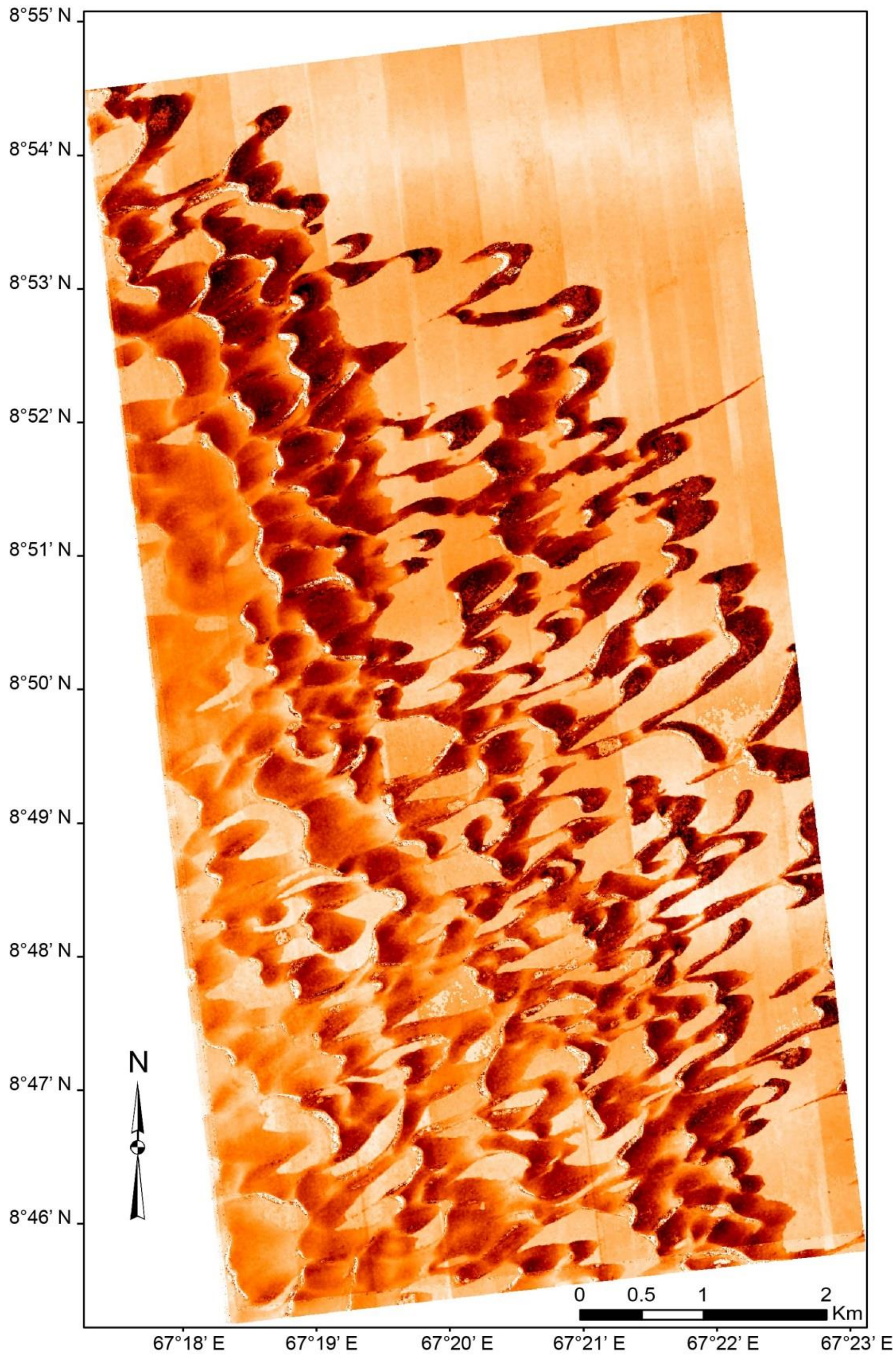

Supplementary Figure 2: First component of the PCA applied to the displacement maps time-series.

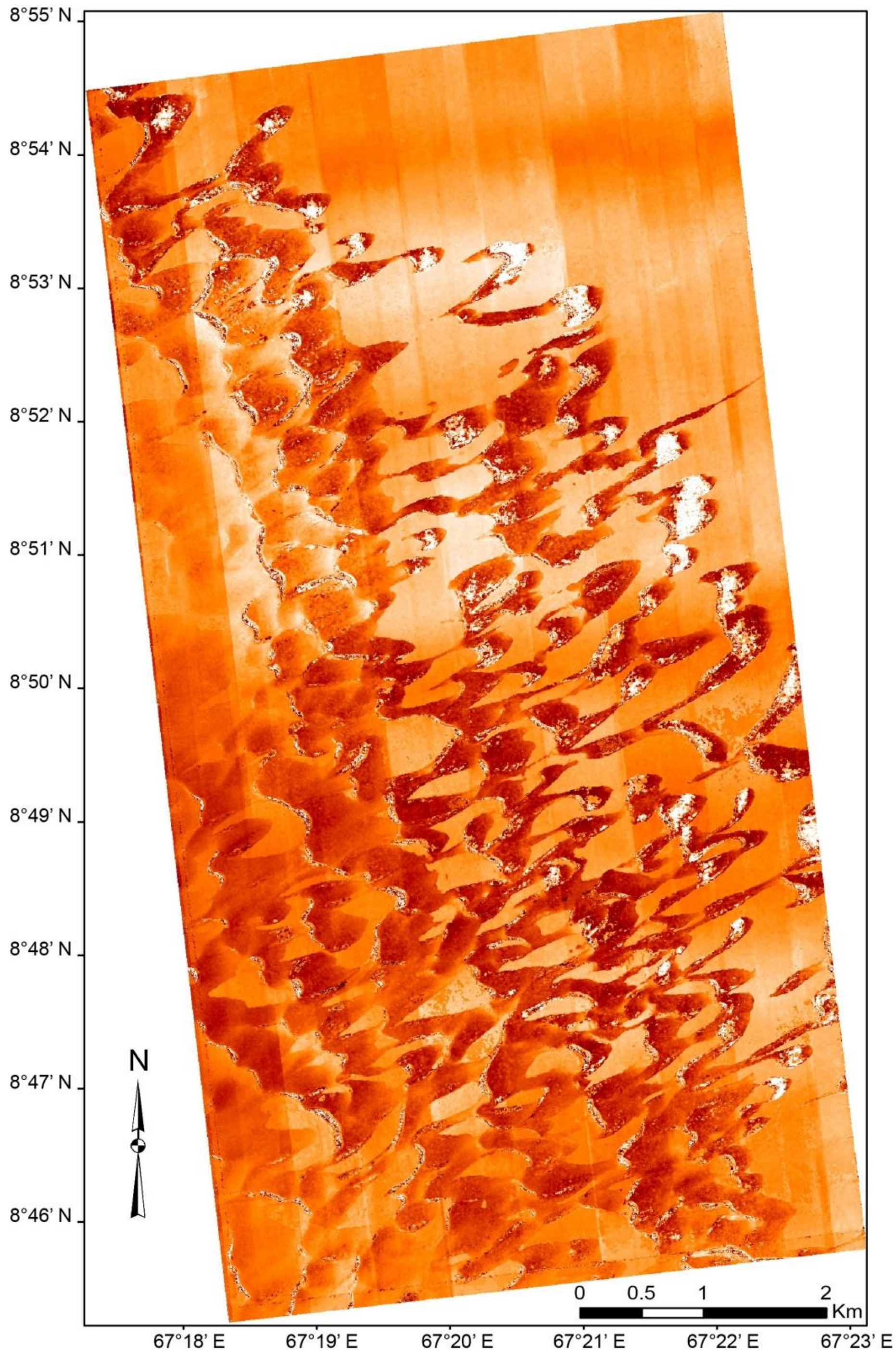

Supplementary Figure 3: Second component of the PCA applied to the displacement maps time-series.

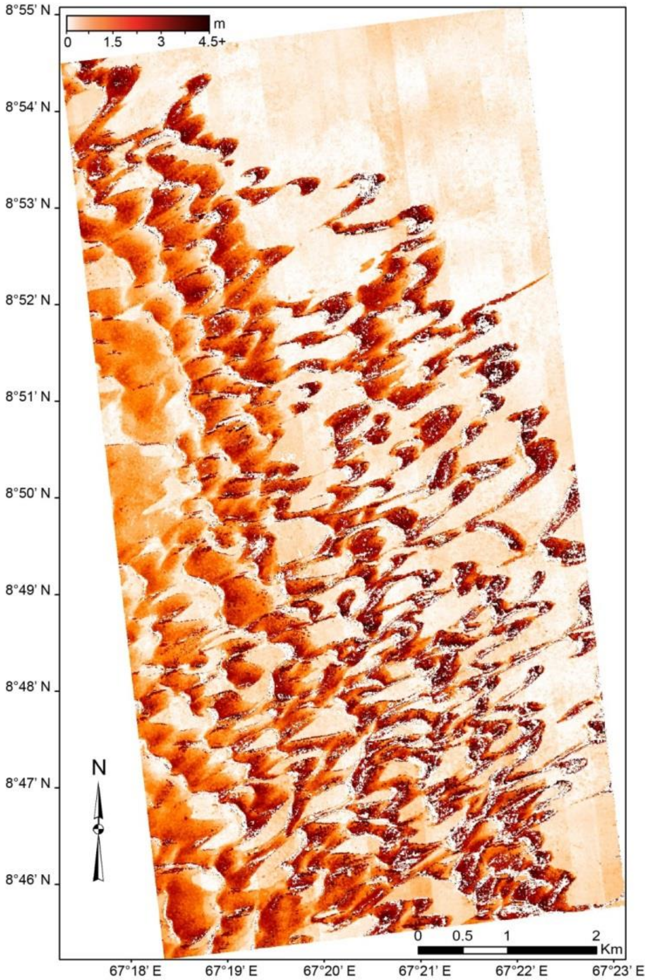

Supplementary Figure 4: Amplitude of the sand ripple displacements in the Nili Patera dune field derived from correlating HiRISE images 18039 and 20729 acquired 209 Earth days apart. The displacement map represented is the composition of the 2 first components (Supplementary Fig. 2,3) of the Principal Component Analysis (PCA) applied to the time-series. Azimuth of the ripples is given in Supplementary Table 1.

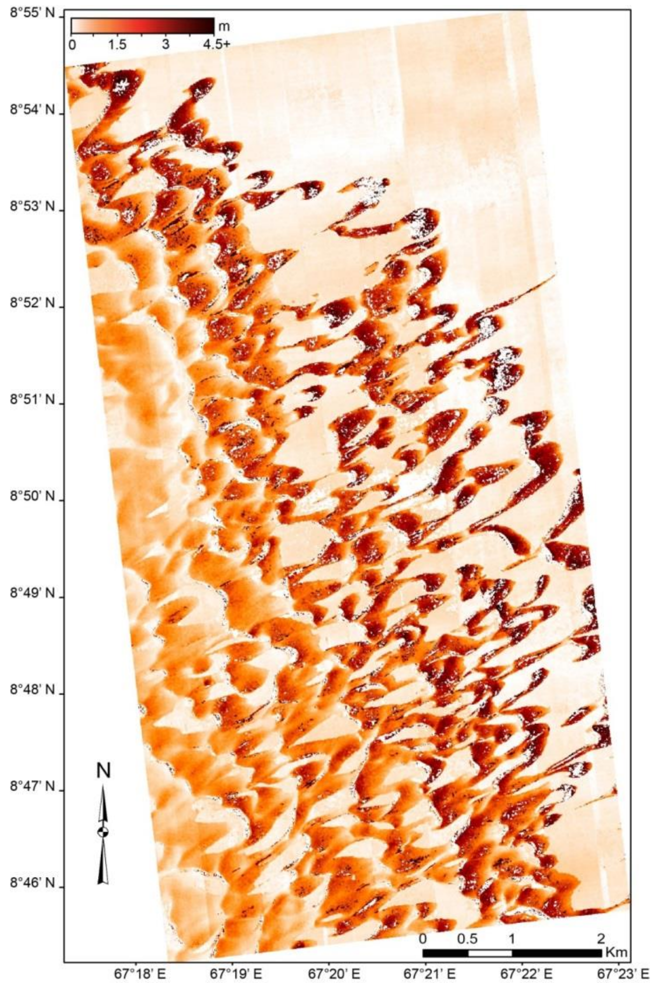

Supplementary Figure 5: Amplitude of the sand ripple displacements in the Nili Patera dune field derived from correlating HiRISE images 20729 and 21625 acquired 72 earth days apart. The displacement map represented is the composition of the 2 first components (Supplementary Fig. 2,3) of the Principal Component Analysis (PCA) applied to the time series. Azimuth of the ripples is given in Supplementary Table 1.

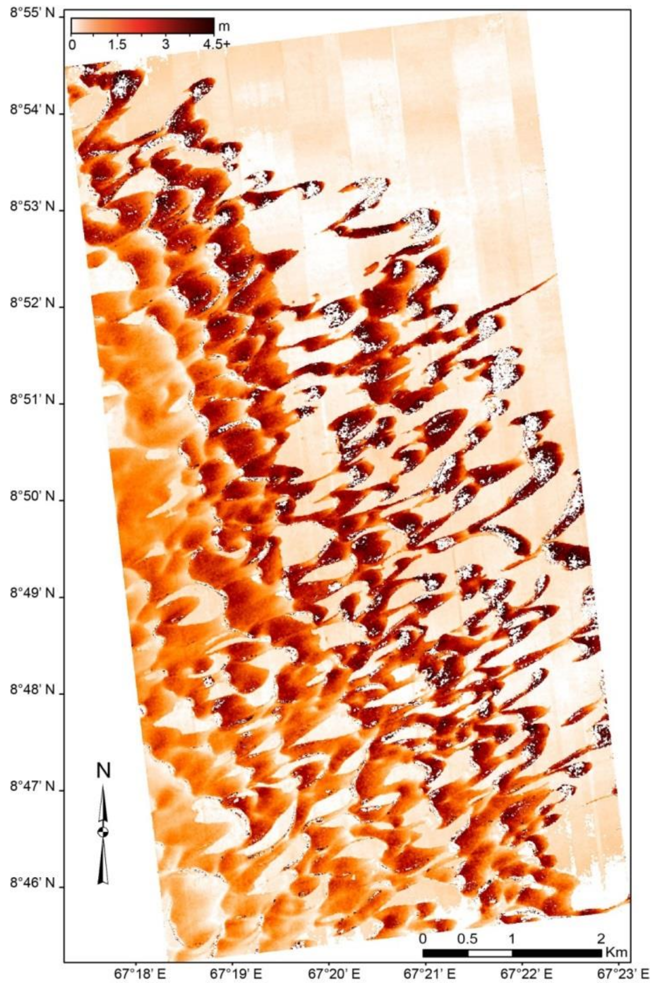

Supplementary Figure 6: Amplitude of the sand ripple displacements in the Nili Patera dune field derived from correlating HiRISE images 21625 and 22364 acquired 56 earth days apart. The displacement map represented is the composition of the 2 first components (Supplementary Fig. 2,3) of the Principal Component Analysis (PCA) applied to the time series. Azimuth of the ripples is given in Supplementary Table 1.

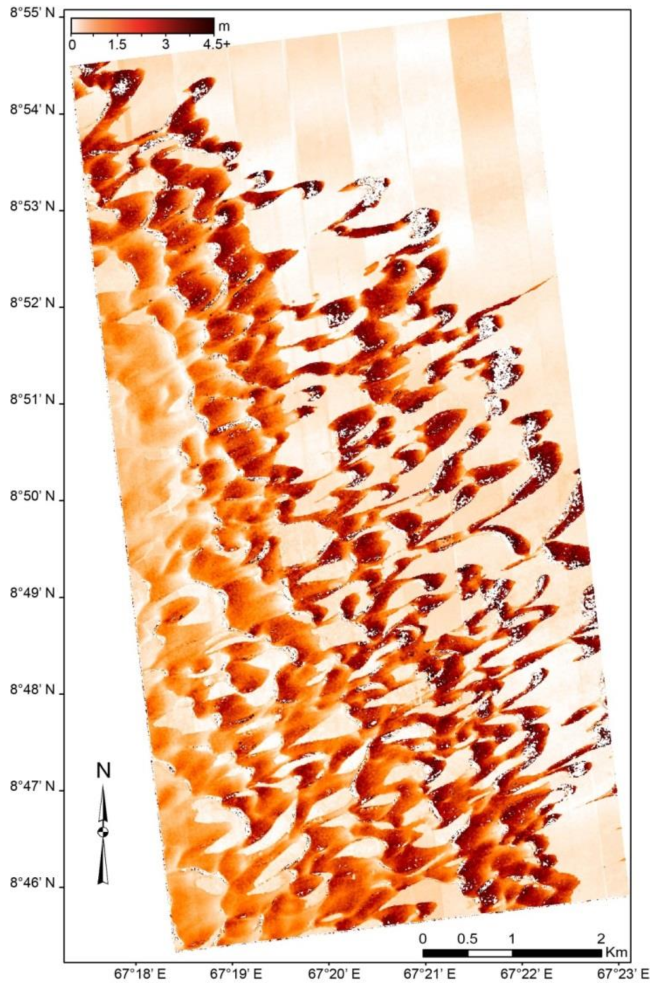

Supplementary Figure 7: Amplitude of the sand ripple displacements in the Nili Patera dune field derived from correlating HiRISE images 22364 and 23142 acquired 60 earth days apart. The displacement map represented is the composition of the 2 first components (Supplementary Fig. 2,3) of the Principal Component Analysis (PCA) applied to the time series. Azimuth of the ripples is given in Supplementary Table 1.

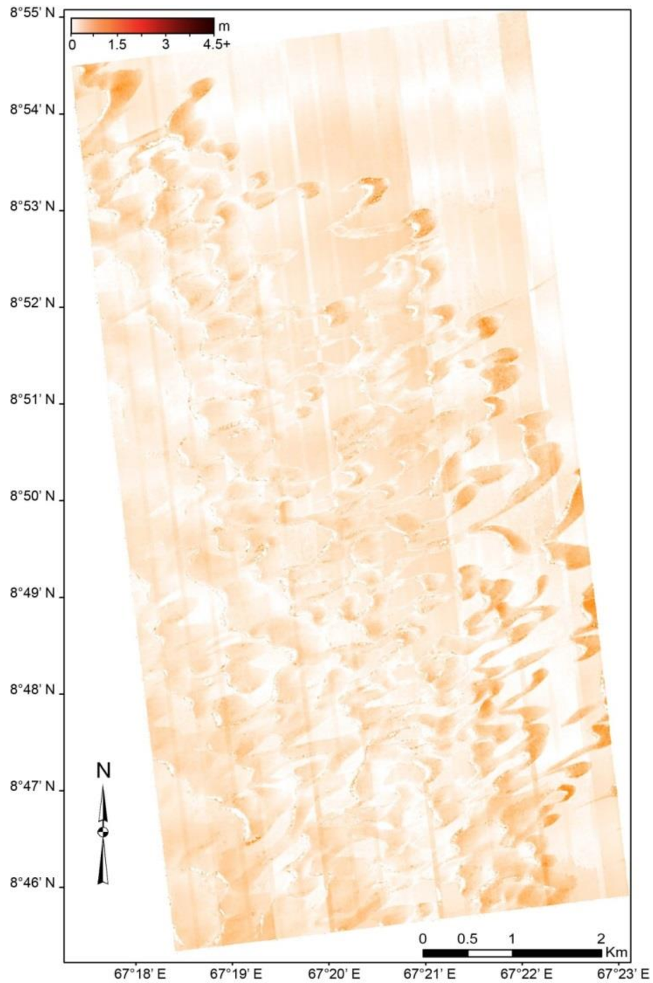

Supplementary Figure 8: Amplitude of the sand ripple displacements in the Nili Patera dune field derived from correlating HiRISE images 23142 and 23353 acquired 17 earth days apart. The displacement map represented is the composition of the 2 first components (Supplementary Fig. 2,3) of the Principal Component Analysis (PCA) applied to the time series. Azimuth of the ripples is given in Supplementary Table 1.

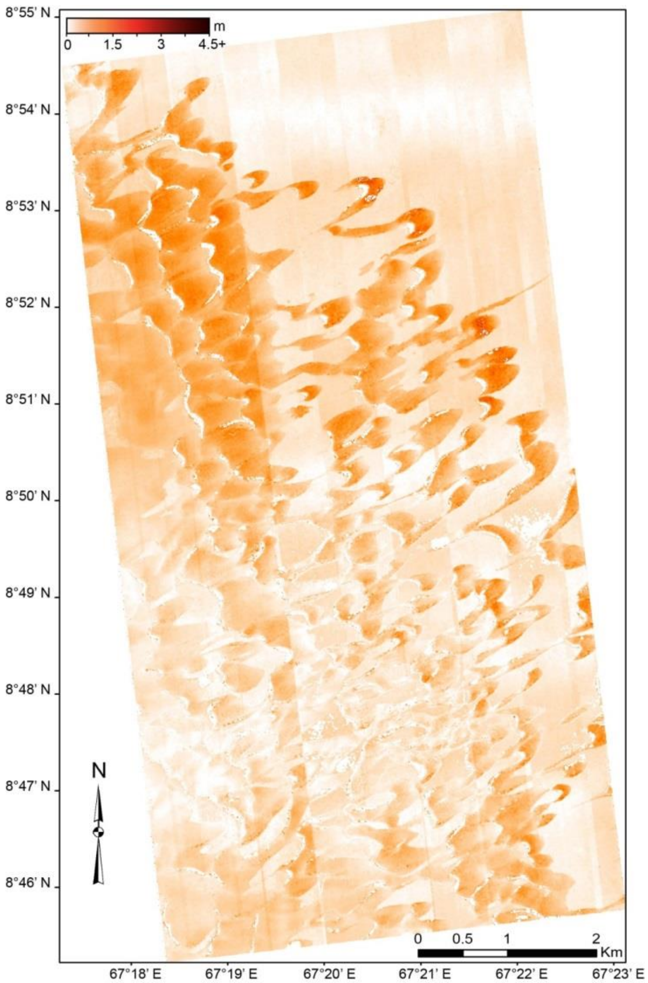

Supplementary Figure 9: Amplitude of the sand ripple displacements in the Nili Patera dune field derived from correlating HiRISE images 23353 and 23564 acquired 16 earth days apart. The displacement map represented is the composition of the 2 first components (Supplementary Fig. 2,3) of the Principal Component Analysis (PCA) applied to the time series. Azimuth of the ripples is given in Supplementary Table 1.

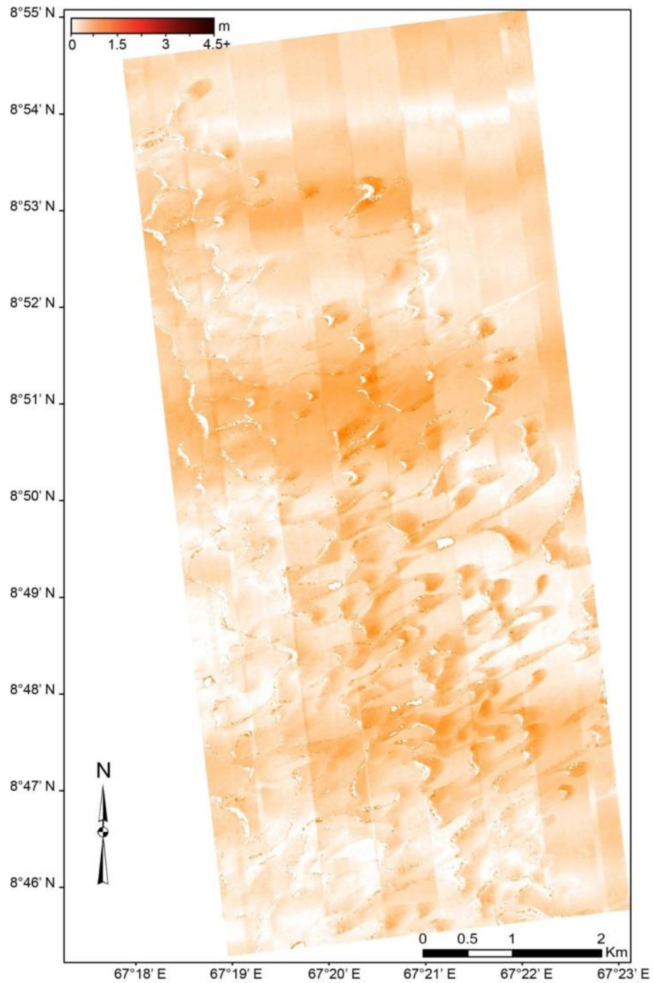

Supplementary Figure 10: Amplitude of the sand ripple displacements in the Nili Patera dune field derived from correlating HiRISE images 23564 and 23920 acquired 28 earth days apart. The displacement map represented is the composition of the 2 first components (Supplementary Fig. 2,3) of the Principal Component Analysis (PCA) applied to the time series. Azimuth of the ripples is given in Supplementary Table 1.

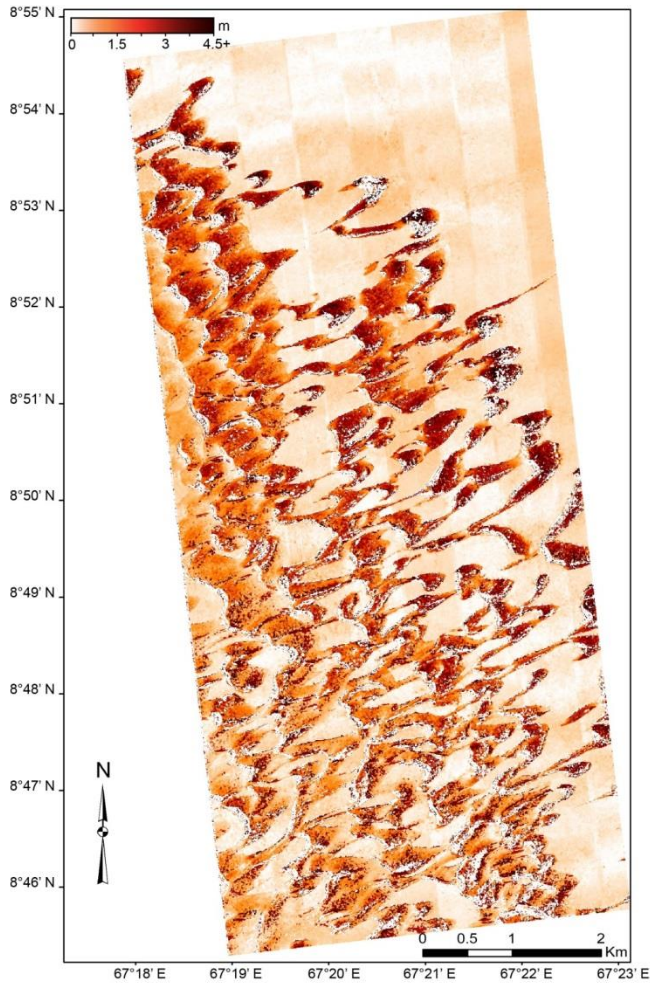

Supplementary Figure 11: Amplitude of the sand ripple displacements in the Nili Patera dune field derived from correlating HiRISE images 23920 and 27032 acquired 242 earth days apart. The displacement map represented is the composition of the 2 first components (Supplementary Fig. 2,3) of the Principal Component Analysis (PCA) applied to the time series. Azimuth of the ripples is given in Supplementary Table 1.

SUPPLEMENTARY TABLE

A	B	C	D	E	F	G	H	I
18039	98.8	06/02/10	-	-	-	-	-	-
20729	206.9	12/28/10	209	8	2.5-23.7	0.42–0.037	0.03-0.02-0.1	120-25.2
21652	251.8	03/10/11	72	5	0.0-28.5	1.16-0.111	0.02-0.01-0.06	110-25.2
22364	286.6	05/05/11	56	17	0.1-21.0	1.77-0.170	0.08-0.04-0.24	110-25.8
23142	322.4	07/04/11	60	4.5	0.0-21.5	1.52-0.136	0.02-0.01-0.06	110-24.8
23353	331.6	07/21/11	17	1	0.1-31.0	0.94-0.083	0.004-0.001-0.01	115-26.7
23564	340.4	08/06/11	16	13.4	0.2-33.2	1.98-0.846	0.06-0.03-0.18	120-43.3
23920	354.85	09/03/11	28	8.5	0.0-33.5	0.73-0.500	0.04-0.02-0.11	145-62.05
27032	105.0	05/02/12	242	5	0.0-18.2	0.29-0.025	0.02-0.1-0.06	110-25.9

Supplementary Table 1: Parameters of HiRISE images composing the time-series. A) Image IDs of the form ESP_0XXXXX_1890 with individual id listed in the column A. B) Solar Longitude (Ls) (degree). C) Acquisition date (mm/dd/yy). D) Number of Earth days between previous and current image. E) Parallax angle between previous and current image (degree). F) Registration residual (average and standard deviation) at the tie-points between the images and the reference image (ESP_018039_1890). G) Reptation sand flux (m^3/m/yr) (mean and error (1-σ)). H) Bias on the ripple displacement (m) due to the use of one unique DEM which does not capture the migration of the dune over time. This error is determined from the difference in emission angle between the two images, the average dune displacement between the DEM acquisition and the image, and the amplitude of the ripple migration, I) Ripple migration orientation (degree from North, positive counter-clockwise) (mode and standard deviation).